Available online at www.sciencedirect.com
SCIENCE DIRECT
Catalysis Today 116 (2006) 74–81
CATALYSIS TODAY
www.elsevier.com/locate/cattod

Nanostructured V-containing hydrotalcite-like materials obtained by non-stoichiometric anion exchange as precursors of catalysts for oxidative dehydrogenation of *n*-butane

Agnieszka Węgrzyn *, Alicja Rafalska-Łasocha, Barbara Dudek, Roman Dziembaj

Faculty of Chemistry, Jagiellonian University, Ingardena 3, Krakow 30 060, Poland

Available online 27 April 2006

Abstract

Hydrotalcite precursors, and subsequently mixed oxide catalysts, with different loadings of vanadium were studied. A modified method of preparation at fixed pH but various amounts of the decavanadate anions below the stoichiometric value, was applied. Different vanadate species as well as carbonates were identified according to XRD patterns and FTIR spectra. The increasing content of vanadium resulted in change of the catalysts properties such as basicity (lower at high V loadings), pore size distribution (pronounced sintering for the highly loaded samples) and the catalytic activity. The highest specific activities were observed for the catalysts with high V content and decreased with decreasing transition metal loading, while the products distribution was more complex, depending both on the basicity and V content.

Keywords: Hydrotalcites; Ion-exchange; Vanadium based catalysts; Butane dehydrogenation

1. Introduction

Hydrotalcites are promising catalysts' precursors since they allow obtaining materials with variable composition and significantly high metal oxide dispersion. Their structure consists of brucite-like layers in which a part of divalent cations (M^{II}) is substituted by trivalent ones (M^{III}). An excessive positive charge is balanced by hydrated anions (A^{n-}) placed between the layers. Thus, general formula of hydrotalcites (HT) may be given as $[M^{II}_{1-x}M^{III}_{x}(OH)_2]A_{x/n}{}^{n-}\cdot zH_2O$. It is possible to change chemical composition of such materials by substitution of metal cations, i.e. Cu^{2+}, Ni^{2+}, Zn^{2+}, Fe^{3+}, Cr^{3+}, or interlayer anions, i.e. $Cr_2O_7{}^{2-}$, $Mo_7O_{24}{}^{6-}$, $V_2O_7{}^{4-}$ [1,2]. Due to hydrotalcites flexibility, the resulting catalysts can be tailored with suitable acid–base and redox properties for studied reaction.

In the present work the usual preparation procedure has been modified. In order to tune transition metal content in the hydrotalcite-like precursor, decreasing amount of vanadate anions available for anion exchange in aqueous solution was used. This allowed us to study the influence of selected parameters on the catalytic activity. Gradual change of vanadium content in the series of the catalysts provided more diverse data than in previously reported study carried out on hydrotalcite-derived mixed oxides [3–6].

2. Experimental

Catalysts' precursors were obtained by ionic exchange of carbonates with decavanadates in the Mg–Al hydrotalcite. Carbonate-containing hydrotalcite with metal ratio Mg/Al close to 2 was prepared using standard co-precipitation method at constant pH. The solution of $Mg(NO_3)_2\cdot 6H_2O$ (51.2 g, 0.2 mol) and $Al(NO_3)_3\cdot 9H_2O$ (37.5 g, 0.1 mol) in 200 ml of distilled water was added drop-wise to 100 ml of aqueous solution of Na_2CO_3 (6.6 g, 0.06 mol). Co-precipitation was carried out at 60 °C under vigorous stirring at pH equal 10.0 ± 0.2. The pH was controlled by simultaneous addition of NaOH (10%). Obtained suspension was stirred for 1 h at 60 °C.

The precipitate, filtered and washed carefully with distilled water, was divided in seven equal portions. Six of them were submitted to ion-exchange (HP8–HP100). The last one (HP0) was used as an undoped reference. The pH equal to 4.5 of an

* Corresponding author. Tel.: +48 12 663 2286; fax: +48 12 634 0515.
E-mail address: wegrzyn@chemia.uj.edu.pl (A. Węgrzyn).

0920-5861/$ – see front matter © 2006 Elsevier B.V. All rights reserved.
doi:10.1016/j.cattod.2006.03.005

approximately 8% hydrotalcite suspension was adjusted using HNO_3 (1:10), then proper amount of decavanadate was added. In the case of complete substitution of CO_3^{2-} by $V_{10}O_{28}^{6-}$ (HP100) 25% excess of the vanadate solution was used. The decavanadate solution was prepared by dissolving 11.7 g of $NaVO_3{\cdot}H_2O$ in 280 ml of H_2O and adjusting the pH to 4.5. Ideally, this procedure should result in the theoretical exchange degree of vanadate for CO_3^{2-} in the range from 0 to 100% of the value required for the complete balancing of the layer charge in the whole series, which is equivalent to 0–30 wt.% of V in the resulting catalysts.

Total time of addition and aging at 60 °C was 1 h. Afterwards the suspensions were filtered, washed with distilled water and dried in air at 60 °C for 18 h. The exchanged HTs were calcined at 700 °C for 13 h in static air to obtain proper catalysts in the form of mixed metal oxides. The hydrotalcite precursors were denoted as HPy while the calcined samples Py. The number (y) in the sample name stands for intended percentage of ion-exchange extent.

Powder X-ray diffraction patterns of the hydrotalcites (precursors) and the hydrotalcite-derived oxides (catalysts) were measured using Philips X'pert PW 3710 diffractometer (Cu Kα radiation, λ = 1.54184 Å), while FTIR spectra were recorded with Bruker IFS 48 spectrometer using the KBr pellet technique. On the basis of XRD data, cell parameters *a* and *c* were calculated from the formulas: $a = 2 \times d_{1\,1\,0}$ and $c = (3 \times d_{0\,0\,3} + 6 \times d_{0\,0\,6})/2$ (for pyrovanadate- and carbonate-rich phase) or $c = (6 \times d_{0\,0\,6} + 9 \times d_{0\,0\,9})/2$ (for decavanadate-rich phase). Additionally, the crystallite size *kc* and *ka* was estimated on the basis of the line broadening using Debye-Sherrer equation: $D = kc = ka = 0.89\ \lambda/(\beta \times \cos\theta)$.

Chemical bulk analysis was performed using elemental analyzer Euro Vector EuroEA 3000 (C, H, N) and XRF spectrometer Oxford 2000 (Mg, Al, V). Using these data several parameters were calculated such as: ion exchange extent (the percentage of the brucite layer charge compensated by $V_{10}O_{28}^{6-}$), difference between expected and obtained Al^{3+} fraction $x = [Al/(Al + Mg)]$ and leaching extent (change of *x*) due to ion exchange.

Textural properties of the calcined materials were studied by means of low temperature N_2 adsorption in ASAP 2010 (Micromeritics) sorptometer. Surface acid and basic properties were determined by temperature-programmed desorption TPD of probe molecules (NH_3 and CO_2, respectively). After outgassing in N_2 flow and cooling down, the flow of NH_3 (1% NH_3/He = 20 ml/min) or CO_2 (85 ml/min) was applied. In the case of carbon dioxide adsorption samples were transferred into desiccator and kept for next 24 h in pure CO_2 atmosphere. Evolution of desorbed molecules was followed by quadrupole mass spectrometer VG SX-200.

Catalytic activity in ODH of *n*-butane was studied in plug-flow microreactor charged with 50 mg of catalysts. After outgassing in N_2 at 550 °C the catalyst bed was fed with reaction mixture (10% n-C_4H_{10}, 10% O_2, 80% N_2, total flow = 100 ml/min) and substrate and products were analyzed on line in GC chromatograph Varian 3400 equipped with TCD and FID detectors.

3. Results and discussion

3.1. Hydrotalcite-like materials

In the Fig. 1. the X-ray powder diffraction patterns of the hydrotalcites intercalated with lower than stoichiometric amount of decavanadates are shown. Comparison of the spectra with Ref. [7] leads to the conclusion that all of the obtained samples had rhombohedral symmetry $3R_1$. The patterns can be divided in two groups: carbonate like patterns characteristic for the samples intercalated by carbonates or other small anionic species (HP0–HP20) and decavanadate-like typical for the hydrotalcites pillared with large anions (HP40–HP100).

In the first group basal reflections (0 0 l) are situated in the same range as it is reported for carbonate hydrotalcites. For the second group significant shift of basal reflection towards lower 2θ degrees was observed as well as presence of side phase, Mg/Al vanadate. In the case of the sample HP40 we claim that both phases, carbonate-rich and decavanadate-rich, coexist. The data collected in Table 1. Show that cell parameter *c* is increasing from 22.98 Å (the value typical for CO_3^{2-}-containing hydrotalcite with high layer charge [2]) to 25.38 Å, probably due to partial intercalation with small vanadate species. Observed depolymerization of decavanadates may occur in diluted solutions [8,9].

Further increase of the amount of decavanadates solution used in the preparation resulted in increase of interlayer distance up to 35.29 Å, which is slightly less than 35.7 Å

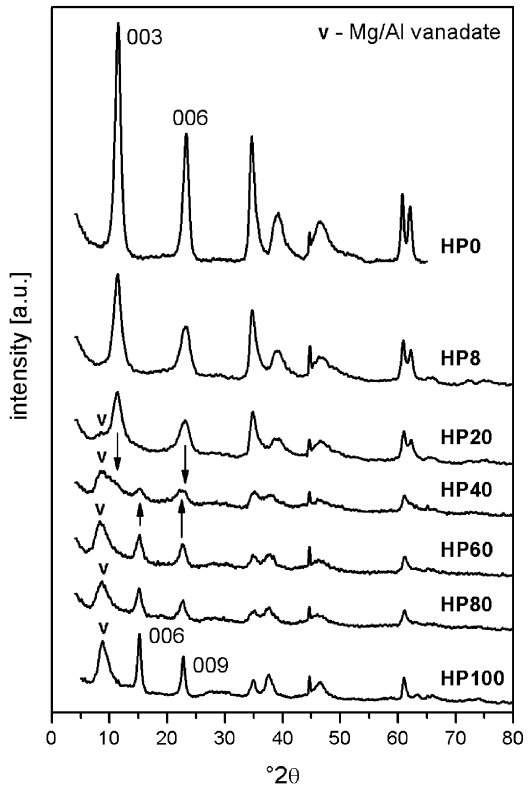

Fig. 1. XRD patterns of not-exchanged sample (HP0) and decavanadate-exchanged hydrotalcites (HP8–HP100).

Table 1
Variation of ion exchange extent, cell parameters and crystallinity of not-exchanged sample (HP0) and decavanadate-exchanged hydrotalcites (HP8–HP100)

Hydrotalcite	Ion exchange extent (%)[a]		Cell parameters (Å)			Crystal size (nm)[b]		
	Intended	Obtained	c_C[c]	c_V[d]	a	kc	Number of layers[e]	ka
HP0	0	0	22.98		3.048	13.7	18	30.8
HP8	8	4.9	23.16		3.042	9.5	12	24.7
HP20	20	11.1	23.31		3.038	8.2	10	24.4
HP40	40	30.5	25.38	34.85	3.034	–	–	24.0
HP60	60	38.3		35.23	3.035	13.3	11	20.2
HP80	80	46.7		35.29	3.031	14.3	12	18.4
HP100	100	64.1		35.08	3.035	21.6	18	21.5

[a] Percentage of layer charge compensated by $V_{10}O_{28}^{6-}$; obtained values of ion exchange extent were calculated on the basis of chemical composition of the catalysts (Al/V ratio).
[b] Calculated using Debye-Sherrer equation.
[c] Dominant interlayer anion CO_3^{2-}, $c = (3d_{0\,0\,3} + 6d_{0\,0\,6})/2$.
[d] Dominant interlayer anion $V_{10}O_{28}^{6-}$, $c = (6d_{0\,0\,6} + 9d_{0\,0\,9})/2$.
[e] Number of layers per crystallite parallel to z-axis.

usually ascribed to $V_{10}O_{28}^{6-}$ with its C_2 axis oriented parallel to the brucite-like sheets [10–12]. The reason that cell parameter c did not reach values typical for pyro- and decavanadate-pillared materials could be high trivalent metal content and consequently strong interactions between brucite-like layers and anions. Progressive deterioration of the structure, due to dissolution in acidic conditions, resulted also in the decrease of the cell parameter a. In such conditions mainly Mg^{2+} cations, having bigger ionic radius than Al^{3+}, are extracted from the hydroxide layers.

The crystallite size ka remain almost unchanged for all of the samples immersed in acidic solution (HP8–HP100) while small discrepancies in kc values (HP8–HP80) may be assigned to overlap of basal reflections of coexisting carbonate- and vanadate-rich phases. It was observed that the crystallites of vanadate-free (HP0) and carbonate-free (HP100) samples consist of the same number of layers, but the crystallite thickness increases due to successful intercalation of $V_{10}O_{28}^{6-}$.

Two phenomena concerning the extent of ion-exchange are worth mentioning. Firstly, for all vanadate-exchanged samples the obtained values were lower than intended. This is caused by repulsion between large decavanadate anions and strong interactions between the layers and anions. Both mechanisms lower the intercalation efficiency. Secondly, complete substitution of CO_3^{2-} by $V_{10}O_{28}^{6-}$ is not essential to obtain pillared nanostructure. Expanded interlayer distance was observed even when only 38 % of required decavanadates were introduced (HP60).

In infrared spectra (Fig. 2.) of the series of hydrotalcites several bands were assigned to OH^- stretching vibrations (≈3450 cm^{-1}) as well as bending modes of interlayer water molecules (≈1626 cm^{-1}) [13]. Although low pH of ion-exchange was applied, modes assigned to CO_3^{2-} were present in the samples HP8, HP20, HP40 and even HP60. However, the higher amount of vanadates was used the lower intensity of following bands was observed: 1360/1404 cm^{-1} (ν_3 stretching CO_3^{2-}), 3035 cm^{-1} (bridging CO_3^{2-}–H_2O) [13]. On the other hand, decavanadate modes became more intensive in the same order (HP40, HP60, HP80, HP100): 964 cm^{-1} (symmetric stretching vibrations of VO_2 or terminal V=O), 812 and 516 cm^{-1} (antisymmetric and symmetric stretching vibrations in V–O–V chains), 740 cm^{-1} (stretching V–O) and 676 cm^{-1} ($H_xV_{10}O_{28}^{6-x}$, x = 1–3) [14–16].

3.2. Calcined materials

Chemical composition of the studied catalysts is shown in Table 2. As explained above, the actual extent of ion-exchange in all samples was lower than expected. Nevertheless, the

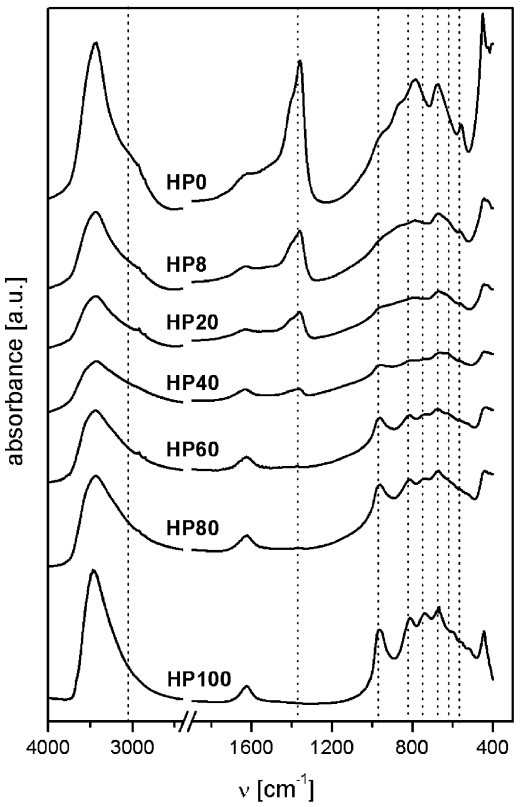

Fig. 2. FT-IR spectra of not-exchanged sample (HP0) and decavanadate-exchanged hydrotalcites (HP8–HP100).

Table 2
Chemical composition of V-doped catalysts

Catalyst	Chemical composition (wt.%)			Molar ratio $x = [Al/(Al + Mg)]$	Deficiency of x (%)[a]	Leaching extent (%)[b]
	Mg	Al	V[c]			
P0	36.1	21.2	0.0 (0)	0.346	3.9	–
P8	30.8	22.6	3.5 (5)	0.397	19.2	12.9
P20	28.4	21.0	7.3 (10)	0.400	20.0	13.4
P40	21.6	17.8	17.1 (18)	0.426	27.9	18.8
P60	21.6	15.9	19.2 (23)	0.399	19.6	13.1
P80	19.7	14.9	21.9 (27)	0.406	21.8	14.7
P100	18.9	12.5	25.2 (30)	0.373	12.0	5.1

[a] Difference between expected (0.333) and obtained value.
[b] Change of x after anion exchange with respect to precursor.
[c] Intended values in parentheses.

applied preparation method provided series of mixed oxides with wide range (from 3.5 to 25.2 wt.%) of transition metal content. Chemical analysis confirmed altered metal cations ratio and increase of Al^{3+} fraction (x). Leaching of Mg^{2+} in V-doped samples with respect to reference material (P0) reached 18.8%.

Structural study (Fig. 3.) of hydrotalcite-derived catalysts with low V-loading (P8, P20) showed mainly quasi-amorphous phase of MgO (periclase), but in comparison to undoped catalyst (P0) there were also traces of another phase. Weak reflections at 20°, 31°–32° and 58° 2θ were assigned to dispersed vanadate phase, probably $Mg_3V_2O_8$. With increasing V-loading more sharp peaks were observed as a result of increasing crystallinity of the studied catalysts. The structure of the sample P40 consisted of three different species: MgO, $Mg_3V_2O_8$ and α-$Mg_2V_2O_7$. The mixture of MgO and α-$Mg_2V_2O_7$ was identified for the samples P60, P80 and P100. These results are consistent with characteristics of Mg- and V-containing hydrotalcite-derived catalysts and with the phase diagram of mixed oxide systems Mg–V–O [4,17–20].

For the selected samples FTIR spectra were recorded (Fig. 4.). With increasing the crystallinity of the samples sharp, well-resolved bands were observed. For the sample P80, with high V content and α-$Mg_2V_2O_7$ structure, modes characteristic for pyrovanadates were assigned at 971–976, 919, 875, 848, 822 cm^{-1}. For the sample with low V-loading (P20) bands at 970, 918, 823, 492 and 470 cm^{-1} were ascribed to orthovanadate. It should be stressed that both assignments are only tentative due to not well resolved bands in both spectra

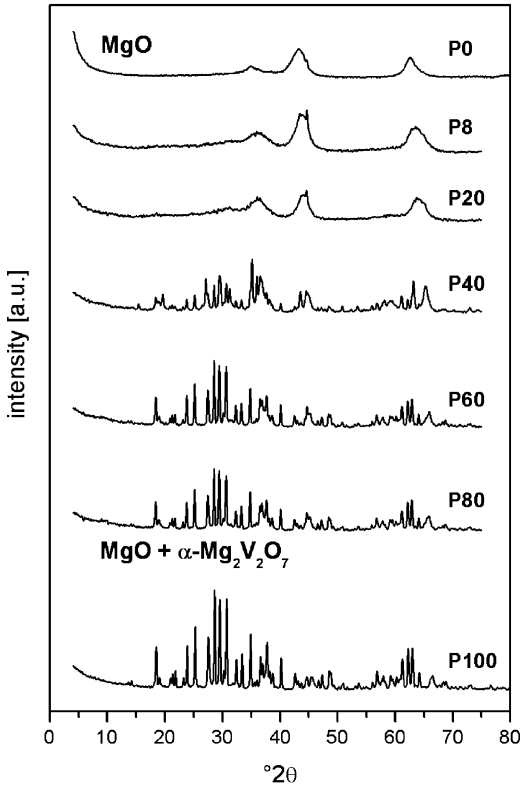

Fig. 3. XRD patterns of V-doped hydrotalcite-derived catalysts.

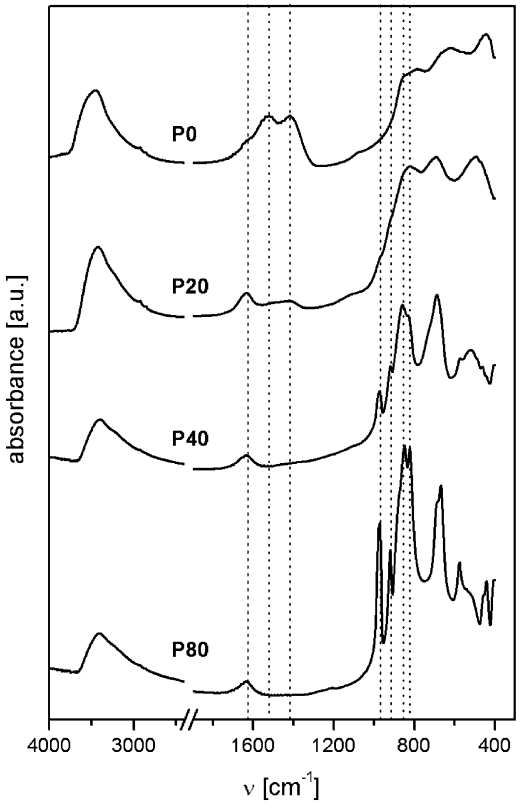

Fig. 4. FT-IR spectra of V-doped hydrotalcite-derived catalysts.

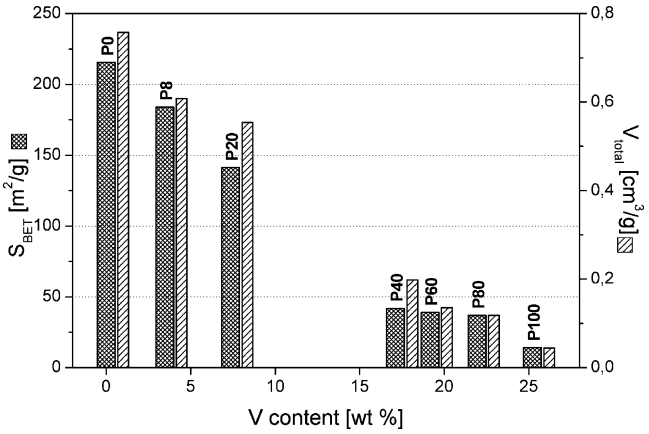

Fig. 5. Surface areas and total pore volumes as function of vanadium content of V-doped hydrotalcite-derived catalysts.

and proximity of diagnostic modes [17,21–23]. For the sample P40 several overlapping bands were found (971–977, 918, 859, 848, 848, 833, 490, 462 cm^{-1}), thus neither pyrovanadate nor orthovanadate cannot be excluded.

Two of the studied samples, P0 and P20, showed ability of CO_2 adsorption when contacted with air. On the catalysts surface bicarbonates (ν_{as}: 1651/1658 cm^{-1}), bidentate carbonates (ν_{as}: 1616/1628–1638 cm^{-1}) and unidentate carbonates (ν_{as}: 1525/1500–1547 cm^{-1}, ν_s: 1420/1400–1430 cm^{-1}) [24] were formed.

The main parameter that was altered within the series of the catalysts was vanadium content. As shown in Fig. 5. and Table 3, both textural parameters S_{BET} and total pore volume decrease gradually with increasing V-loading, from 216 m^2/g and 0.757 cm^3/g to 14 m^2/g and 0.044 cm^3/g for undoped (P0) and highly loaded (P100) catalysts, respectively. Continuous sintering of pores in the same order (P0–P100) is shown in Fig. 6. In the first stage the smallest pores (≈1.6 nm) disappear, then bigger ones (≈6.0 and ≈10.0 nm) and in the end non-porous solid is formed (P100). Hysteresis loops (Fig. 7) [25,26] for all of the catalysts indicated the presence of bottle-shaped pores.

Concentration of basic sites responsible for CO_2 adsorption observed in FTIR spectra were measured by means of CO_2-TPD (Table 4.). Highly basic (678.8 μmol CO_2/g, 3.148 μmol CO_2/m^2) undoped catalyst P0 contains at least two groups of basic sites of different strength; maximum desorption rate was

Table 3
Surface areas, total pore volumes and pore size distribution of V-doped catalysts

Catalyst	Textural properties		Maxima of pore diameter distribution (nm)
	S_{BET} (m^2/g)	V_{total} (cm^3/g)	
P0	216	0.757	1.6, 6.4
P8	184	0.608	1.6, 5.3
P20	141	0.554	(1.5), 5.9
P40	42	0.198	9.8
P60	39	0.136	12.7
P80	37	0.118	11.5
P100	14	0.044	(1.7), (16.9)

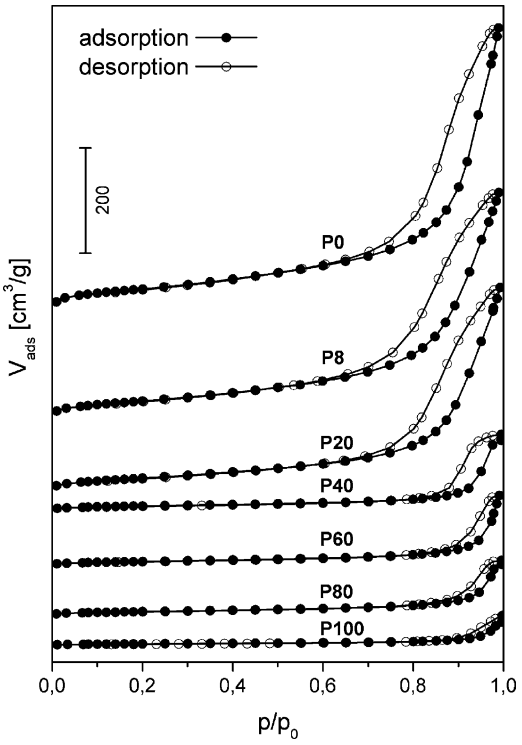

Fig. 6. Adsorption–desorption isotherms obtained on V-doped hydrotalcite-derived catalysts.

observed at 167 °C and 270 °C (Fig. 8.). Carbon dioxide was desorbed from the surface of the two catalysts doped with smallest portions of vanadium, P8 and P20, in the same temperature range but in lower amount. In this case new strong

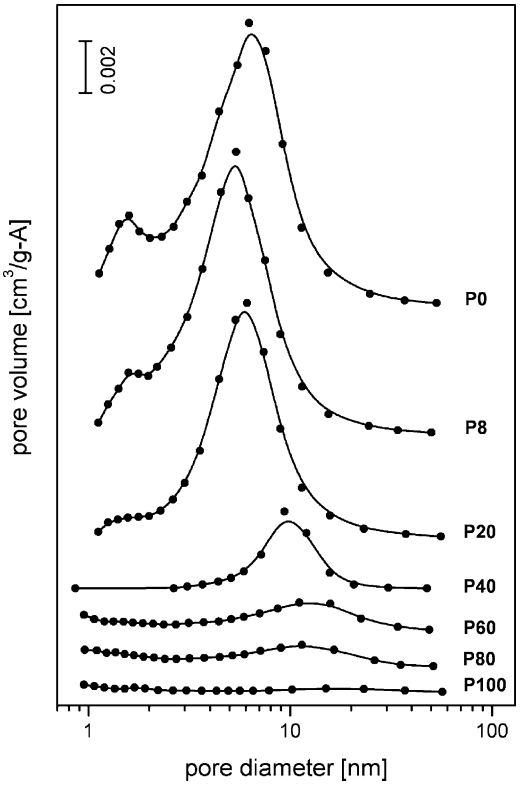

Fig. 7. Pore size distribution for V-doped hydrotalcite-derived catalysts.

Table 4
Densities and number of acid and basic sites obtained in NH_3-TPD and CO_2-TPD on V-doped catalysts

Catalyst	Density (μmol/m^2)		Amount (μmol/g)		Coverage (% of S_{BET})	
	NH_3	CO_2	NH_3	CO_2	NH_3[a]	CO_2[b]
P0	0.452	3.148	97.5	678.8	1.50	27.19
P8	1.233	2.527	226.9	464.9	4.10	21.82
P20	1.285	1.971	181.6	278.6	4.27	17.02
P40	1.380	1.120	57.6	46.8	4.60	9.67
P60	1.375	0.520	53.6	20.3	4.57	4.49
P80	0.372	2.219	13.7	81.7	1.24	19.16
P100	1.452	8.318	20.5	117.4	4.82	71.82

[a] Cross-sectional area of NH_3 = 0.05515 nm^2.
[b] Cross-sectional area of CO_2 = 0.14336 nm^2.

basic sites with maximum desorption rate at 467–464 °C were formed. We assume that introduced vanadium ions modify properties of already existing basic sites rather than give rise to creation of new ones.

Further increase in the V-content from P40 to P100 did not change significantly the strength of basic sites, from which desorption occurs at temperatures between 140 and 470 °C, but reduced their quantity. Generally, the quantity of basic sites decreased to 20.3 μmol CO_2/g and basic sites density to 0.520 μmol CO_2/m^2 in the group of the catalysts P0–P60. High values of both parameters were observed for the last two high-crystalline samples, P80 and P100. It cannot be excluded that in described experiments not only chemisorption was observed but a part of adsorbed CO_2 formed bulk carbonates. Nevertheless, similar basic sites densities were reported elsewhere for the Mg/Al hydrotalcite-derived mixed oxides [27,28].

Much lower quantities of adsorption sites on the surface of the catalysts P0–P8–P20 were measured using basic probe molecule NH_3; 97.5, 226.6, 181.6 μmol NH_3/g, respectively. For the rest of the studied samples amounts of adsorbed ammonia were even smaller, ranging from 57.6 μmol NH_3/g for P40 to 13.7 μmol NH_3/g for P80. Although decreasing quantities of ammonia per mass unit were desorbed in the catalysts with increasing V-loading, the introduction of vanadium enhances the acid sites density. Value of this parameter is similar for most of the V-doped samples and equal 1.2–1.4 μmol NH_3/m^2. Consequently, the coverage of the surface almost does not change and is close to 4%. NH_3 desorption profiles shown in Fig. 9 do not have as rich structure as in the case of CO_2. Broad asymmetric peaks start at around 100 °C and their maxima are in the range of 205–254 °C for the samples P0–P60 and 157–177 °C for P80–P100. The shape of desorption peaks indicate the influence of diffusion effects and probable re-adsorption of molecules.

3.3. Catalytic study

Modification of the hydrotalcites preparation procedures applied in present work gave the opportunity to study the influence of the transition metal loading on the activity and selectivity in ODH of *n*-butane. In this case the influence of other preparation parameters, in particular pH of ion exchange strongly affecting the metal ratio in the brucite-like layers, could be neglected.

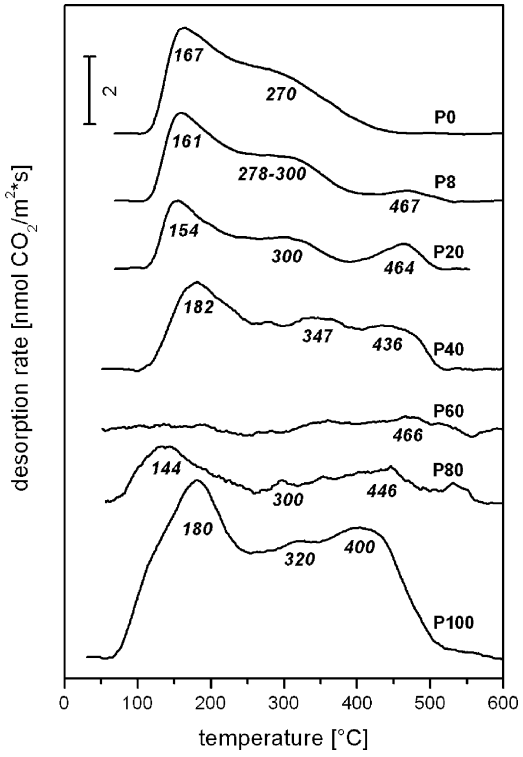

Fig. 8. CO_2 desorption profiles for V-doped hydrotalcite-derived catalysts.

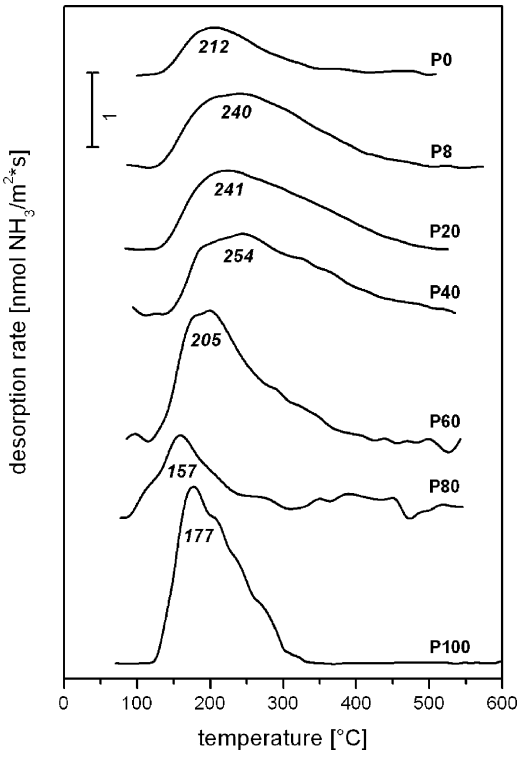

Fig. 9. NH_3 desorption profiles for V-doped hydrotalcite-derived catalysts.

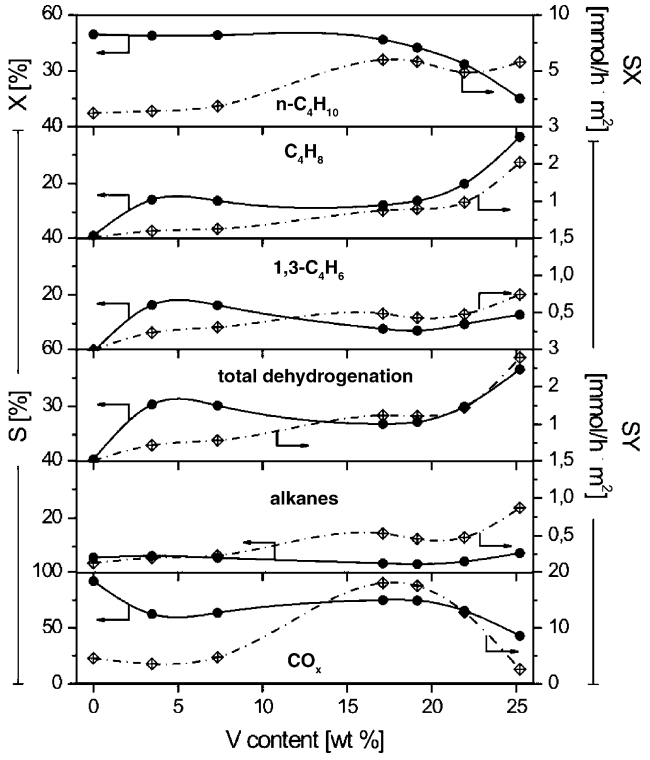

Fig. 10. Activities and selectivities of V-doped hydrotalcite-derived catalysts in ODH of *n*-butane (X: conversion, S: selectivity, SX, SY: specific activity and specific yield [mmol/h m^2]).

Conversion of *n*-butane (Fig. 10.) for the undoped Mg/Al mixed oxides (P0) as well as the catalysts with the smallest V loadings was around 50%. It decreased subsequently to 15% (P100) when higher quantities of transition metal were present. On the other hand, total selectivity to dehydrogenated products increased from 2% (P0) to 31% (P8). Further increase of V loading brought about slight decrease of this parameter (S_{ODH} = 22–19% for P20–P40–P60) and again increase for the last two samples (S_{ODH} equal 30 and 50% for P80 and P100, respectively).

There were also observed products of undesired reactions such as cracking and total oxidation. Selectivity to alkanes was not higher then 8% within the whole series. CO_x was formed with selectivity lower than 50 % only for one catalyst (P100). Significant selectivity to carbon oxides was observed for the other V-doped catalysts ($S_{CO_x} = 62 - 75\%$) as well as undoped one ($S_{CO_x} = 92\%$).

Opposite trend was obtained for specific activity SX. High crystalline samples P40–P100 are more active than amorphous ones, P0–P20. Specific yield of dehydrogenation products (SY_{ODH}) follows the same trend as specific activity. The highest yield of CO_x was found for the high crystalline samples with medium V loading (P40–P80).

The most efficient catalysts showed high activity (X) and selectivity towards desired products (ODH) with relatively low selectivity to CO_x at the same time. This applies to low crystalline catalysts with the structure of MgO containing dispersed vanadate phase (P8–P20). On the other hand, catalyst with the structure of α-$Mg_2V_2O_7$ (P100) was very selective in ODH. The performance of the two first mentioned catalysts (P8–P20) can be additionally enhanced by lowering the conversion of alkane and by blocking consecutive reactions, mainly total oxidation.

Comprehensive explanation of obtained results requires detailed analysis of structural, redox and acido–basic properties of the catalysts. In majority of papers dealing with Mg–V–O oxide catalysts for ODH of alkanes, magnesium orthovanadate $Mg_3V_2O_8$ is recognized as active and selective phase. Pyrovanadate α-$Mg_2V_2O_7$ or metawanadate MgV_2O_6 are responsible for deep oxidation, mainly CO_x [29–31].

Orthovanadate or low crystalline MgO with VO_4 tetrahedra lowers the amount of available oxygen ions. Oxygen atoms from pyrovanadate, in which VO_4 tetrahedra share the corners, are easily released to take part in the reaction according to Mars-van Krevelen mechanism. Thus, the correlation between reducibility and catalytic activity was proposed—the easier reducibility of the cation, the lower selectivity to ODH products is observed [32,33]. For this reason, the catalyst containing isolated VO_4 groups should be more difficult to reduce than α-$Mg_2V_2O_7$ and MgV_2O_6. Nevertheless, results reported by Chang et al. [34] showed that such materials (similar to the samples P8 and P20) were easily reduced at temperatures lower than used for pyrovanadate (e.g. P100).

To fully explain obtained results, another mechanism must be taken into account. Due to relatively high electronegativity of Mg, oxygen atom in Mg–O–V unit is more nucleophilic (basic) than in correspondent V–O–V units. According to mechanism described by Bielański and Haber [35,36], nucleophilic oxygen anions activate hydrocarbon molecule by hydrogen abstraction. Electrophilic (acidic) oxygen anions, such as in V–O–V units, lead to total oxidation.

Products distribution can be explained on the basis of acido–basic character of the catalysts. Highly basic catalysts favor desorption of alkenes and thus consecutive reaction are stopped [29,30,37]. Enhanced production of CO_x on P40 and P60 catalysts might be due to their high acid sites density, while products desorption from highly acidic and highly basic surface of P8–P20 catalysts occurs when 1,3-butane is formed in significant amount.

Additional information concerning reaction mechanism is provided by analysis of butene isomers distribution. The most probable route of butane activation is formation of secondary butyl radical. This hypothesis is based on observed 1-butene:*cis*-2-butene:*trans*-2-butene ratio close to 2.6:1.0:1.0 for highly V-loaded catalysts. For the catalysts with vanadium content lower than 10 wt.% this ratio is close to 2.0:1.0:1.0, which is still different from equilibrium ratio (1.0:1.0:1.1) [30].

Specific activity and specific yield of dehydrogenated products in general depend on vanadium content. It should be noted however, that other effects may play important role in the description of the studied mechanism. For example, synergy between different phases present in P8–P20 (MgO and orthovanadate), P40–P100 (ortho- and pyrovanadate). Enhancement of catalytic performance due to such phenomenon was reported for Mg–V–O oxide catalysts studied in ODH of propane [38].

4. Conclusions

Application of lower than stoichiometric amount of vanadates during intercalation procedure resulted in formation of the structure typical for the hydrotalcites pillared by mixture of carbonates and small vanadate anions and/or decavanadates. At low percentage of ion-exchange, a mixture of various anionic species was observed due to depolymerization of decavanadates in diluted solutions.

In the course of the calcination mixed metal oxides were formed; however, the phase composition depended on vanadium content. For the samples with ion-exchange up to 20% mainly periclase (MgO) phase was identified. The hydrotalcites with high vanadate content after calcination consisted of the mixture of MgO and α-$Mg_2V_2O_7$.

The surface area of the catalysts varied from 216 to 14 m^2/g and the pore volume from 0.757 to 0.044 cm^3/g for the lowest and the highest vanadium content in the sample, respectively. Bottle-shaped mesopores with diameter around 6 nm were identified in samples with small V-loading. The increase of vanadium content to 25 wt.% caused formation of nearly non-porous solid.

Surface acidity per surface unit increases in V-doped catalysts with respect to undoped reference sample and remains constant for most of the samples. Total basicity per surface unit as well as per gram decrease in the case of V-doped samples (up to 19 wt.%) and then slightly increases for the samples with the highest V-loading.

Specific activity of the studied catalysts also depends on V-content. The higher amount of V is introduced, the more butane molecules reacts per surface area unit. The highest selectivities to ODH products (up to 31%) and simultaneously the lowest selectivity in burning to CO_x were observed for the two catalysts with the smallest V content. Nevertheless, the specific yield of ODH products per surface unit was highest for the catalysts with V-loading in the range of 17–25 wt.%. Decrease of 1,3-butadiene selectivity at high V-loading should be related to the presence of the high crystalline α-$Mg_2V_2O_7$. Both acid and basic sites are necessary for high activity and selectivity in ODH of *n*-butane; however, total selectivity for the dehydrogenated products was higher on the highly basic catalysts.

Acknowledgement

Financial support of the State Committee for Scientific Research (4 T09A 135 25) is kindly acknowledged.

References

[1] S. Miyata, US Patent. 796,792 (1974).
[2] F. Cavani, F. Trifirò, A. Vaccari, Catal. Today 11 (1991) 173.
[3] G. Carja, R. Nakamura, T. Aida, H. Niiyama, J. Catal. 218 (2003) 104.
[4] K. Bahranowski, G. Bueno, V. Cortés Corberán, F. Kooli, E.M. Serwicka, R.X. Valenzuela, K. Wcisło, Appl. A 185 (1999) 65.
[5] R. Dula, K. Wcisło, J. Stoch, B. Grzybowska, E.M. Serwicka, F. Kooli, K. Bahranowski, A. Gaweł, Appl. A 230 (2002) 281.
[6] M.J. Holgado, F.M. Labajos, M.J.S. Montero, V. Rives, Mater. Res. Bull. 38 (2003) 1879.
[7] S.P. Newman, W. Jones, P. O'Connor, D.N. Stamires, J. Mater. Chem. 12 (2002) 153.
[8] J. Livage, Coord. Chem. Rev. 178 (1998) 999.
[9] J.C. Bailar, H.J. Emeléus, R. Nyholm, A.F. Trotman-Dickenson, Comprehensive Inorganic Chemistry, 519, Pergamon Press, Oxford, 1973.
[10] M.A. Drezdon, Inorg. Chem. 27 (1988) 4628.
[11] V. Rives, M.A. Ulibarri, Coord. Chem. Rev. 181 (1999) 61.
[12] T. Kwon, G.A. Tsigdinos, T.J. Pinnavaia, J. Am. Chem. Soc. 110 (1988) 3653.
[13] J.T. Kloprogge, D. Wharton, L. Hickey, R.L. Frost, Am. Mineral. 87 (2002) 623.
[14] F. Kooli, V. Rives, M.A. Ulibarri, Inorg. Chem. 34 (1995) 5114.
[15] M.A. Ulibarri, F.M. Labajos, V. Rives, R. Trujillano, W. Kagunya, W. Jones, Inorg. Chem. 33 (1994) 2592.
[16] E. López-Salinas, Y. Ono, Bull. Chem. Soc. Jpn. 65 (1992) 2465.
[17] D. Siew Hew Sam, V. Soenen, J.C. Volta, J. Catal. 123 (1990) 417.
[18] S. Köbel, D. Schneider, C.Chr. Schüler, L.J. Gauckler, J. Eur. Ceram. Soc. 24 (2004) 2267.
[19] G.M. Clark, R. Morley, J. Solid State Chem. 16 (1976) 429.
[20] M. del Arco, M.J. Holgado, C. Martin, V. Rives, J. Mater. Sci. Lett. 6 (1987) 616.
[21] J.M. López Nieto, A. Dejoz, M.I. Vázquez, Appl. Catal. A 132 (1995) 41.
[22] F.M. Labajos, V. Rives, P. Malet, M.A. Centeno, M.A. Ulibarri, Inorg. Chem. 35 (1996) 1154.
[23] X. Gao, P. Ruiz, Q. Xin, X. Guo, B. Delmon, Catal. Lett. 23 (1994) 321.
[24] J.I. Di Cosimo, V.K. Díez, M. Xu, E. Iglesia, C.R. Apesteguía, J. Catal. 178 (1998) 499.
[25] G. Leofanti, M. Padovan, G. Tozzola, B. Venturelli, Catal. Today 41 (1998) 207.
[26] K. Kaneko, J. Membr. Sci. 96 (1994) 59.
[27] V.K. Díez, C.R. Apesteguía, J.I. Di Cosimo, J. Catal. 215 (2003) 220.
[28] J. Palomerque, J. Lopez, F. Figueras, J. Catal. 211 (2002) 150.
[29] L.M. Madeira, M.F. Portela, Catal. Rev. 44 (2) (2002) 247.
[30] M.A. Chaar, D. Patel, M.C. Kung, H.H. Kung, J. Catal. 105 (1987) 483.
[31] H.H. Kung, M.C. Kung, Appl. Catal. A 134 (1992) 668.
[32] O.S. Owen, M.C. Kung, H.H. Kung, Catal. Lett. 12 (1992) 45.
[33] D. Patel, P.J. Andersen, M.C. Kung, H.H. Kung, J. Catal. 125 (1990) 132.
[34] W.S. Chang, Y.Z. Chen, B.L. Yang, Appl. Catal. A 124 (1995) 221.
[35] A. Bielański, J. Haber, Oxygen in Catalysis, 131, Marcel Dekker, Nowy York, 1991.
[36] B. Grzybowiska-Świerkosz, Appl. Catal., A: Gen. 157 (1997) 409.
[37] S. Albonetti, F. Cavani, F. Trifirò, Catal. Rev. Sci. Eng. 38 (1996) 413.
[38] X. Gao, P. Ruiz, Q. Xin, X. Guo, B. Delmon, J. Catal. 148 (1994) 56.